arXiv:astro-ph/0612674v1 22 Dec 2006

Massive star formation via high accretion rates and early disk-driven outflows

Robi Banerjee[1,2] and Ralph E. Pudritz[2,3]

[1]*Institute of Theoretical Astrophysics, University of Heidelberg, Albert-Ueberle-Str. 2, 69120 Heidelberg, Germany*

[2]*Department of Physics and Astronomy, McMaster University, Hamilton, Ontario L8S 4M1, Canada*

[3]*Origins Institute, McMaster University, Arthur Bourns Bldg 241, Hamilton, Ontario L8S 4M1, Canada*

ABSTRACT

We present an investigation of massive star formation that results from the gravitational collapse of massive, magnetized molecular cloud cores. We investigate this by means of highly resolved, numerical simulations of initial magnetized Bonnor-Ebert-Spheres that undergo collapse and cooling. By comparing three different cases - an isothermal collapse, a collapse with radiative cooling, and a magnetized collapse - we show that massive stars assemble quickly with mass accretion rates exceeding $10^{-3}\,M_{\odot}\,\mathrm{yr}^{-1}$. We confirm that the mass accretion during the collapsing phase is much more efficient than predicted by selfsimilar collapse solutions, i.e. $\dot{M} \sim c^3/G$. We find that during protostellar assembly the mass accretion reaches $20 - 100\,c^3/G$. Furthermore, we determined the self-consistent structure of bipolar outflows that are produced in our three dimensional magnetized collapse simulations. These outflows produce cavities out of which radiation pressure can be released, thereby reducing the limitations on the final mass of massive stars formed by gravitational collapse. Moreover, we argue that the extraction of angular momentum by disk-threaded magnetic fields and/or by the appearance of bars with spiral arms significantly enhance the mass accretion rate, thereby helping the massive protostar to assemble more quickly.

Subject headings: accretion, accretion discs, magneto-hydrodynamics, ISM: clouds, evolution, methods: numerical

1. Introduction

The formation of massive stars is still a highly debated question. Low mass stars accrete the bulk of their mass through their circumstellar disks before nuclear burning turns on (eg.

Shu et al. (1987)). Massive stars on the other hand, have Kelvin-Helmholtz time scales that are smaller than the dynamical time so that young massive stars start to burn their nuclear fuels while still accreting the surrounding gas (e.g., Yorke 2002, 2004, and references herein). Infall, or flow of gas through a surrounding disk, therefore faces a major obstacle in the form of the radiative pressure that such massive stars will produce as they are still forming.

Early spherical accretion models suggest that the resulting radiation pressure could limit the final mass of the star to $\sim 40\,M_\odot$ if the accretion rate is not high enough ($\gtrsim 10^{-3}\,M_\odot\,\mathrm{yr}^{-1}$) (Kahn 1974; Wolfire & Cassinelli 1987). More recent two dimensional simulations by Yorke & Sonnhalter (2002) showed that the limitations on the final mass of the massive star can be relaxed if accretion through the protostellar disk is included in models of massive star formation. Still, even this result yields mass limits of $\sim 43\,M_\odot$. Krumholz et al. (2005) argued that the effects of radiation pressure are limited by the escape of radiation through an outflow cavity. These results are were based on simulations using Monte-Carlo-diffusion radiative transfer models where the outflow cavities are parameterized by varying opening angles.

Alternatively, massive stars could form through coalescence of intermediate mass stars (Bonnell et al. 1998). This formation process would be starkly different from the formation of low mass stars which assemble quickly through accretion of the molecular gas. So far, observations of the intermediate state of massive star formation are rare and difficult to obtain. Nevertheless, a few massive objects which show evidence for an ongoing accretion process are known by now (Chini et al. 2004; Patel et al. 2005; Chini et al. 2006; Beltrán et al. 2006).

We have developed detailed 3D collapse simulations of magnetized, star forming cores and have shown that outflows and gravitational collapse are inseparably linked. In fact, we found in earlier work on the assembly of low mass stars (e.g., Banerjee & Pudritz 2006) that outflow cavities are carved out of the collapsing envelope very early - much before even a solar mass of material has been assembled into the star. This important early outflow activity we suggested, could play a key role in actually opening up a channel to radiation pressure in the more massive systems. The outflow channel is not imposed by an external model but arises as a natural consequence of the generation of an outflow during the formation of a magnetized disk.

Our first study of massive star formation was in the context of the turbulent fragmentation picture. Specifically, we followed the formation of massive stars in supersonic turbulence by using a 3D, adaptive mesh (AMR) simulation and showed that filamentary accretion plays an important role in focusing the collapse of material onto a massive young star and its disk (Banerjee et al. 2006, henceforth BPA06). We included a full list of coolants and found that the central regions of the collapse behaved somewhat like Bonnor-Ebert spheres. We did not have MHD at work in those calculations.

The present paper follows up on these previous efforts. Instead of trying to track the formation of a massive star in a very large cluster simulation, we concentrate here on the collapse of one massive central region chosen to mimic the massive collapse we found in BPA06. The choice of an initial magnetized Bonnor-Ebert sphere is a reasonable starting point for such a focused-in study. In particular, we study the collapse of a massive molecular cloud core with a total mass of $\sim 170\,M_{\odot}$, which we model as a sphere that is initially in in pressure equilibrium with the surrounding medium i.e. Bonnor-Ebert-Spheres (BE-Spheres).

We shall show that outflows are also an early aspect of the formation of massive stars. We self-consistently determine the initial scale and structure of outflow cavities that are carved by magnetic tower flows that are driven by the forming protostellar disk. In particular we study the influence of radiative cooling and magnetic fields on the collapse of such cloud cores thereby discussing the similarities and differences of these models. We find that these outflows are launched very early, much before the central stars have even accumulated a solar mass worth of material. This means that even before radiation pressure becomes a factor in the formation of a massive star, the outflow has created the cavity out which the radiation pressure, when it eventually appears, can be released. Early outflows therefore, play a central role in the assembly of such stars.

Our paper is organized as follows. In Sec. 2 we describe the numerical modelling and initial conditions of our simulations. We discuss the accretion process and rates in Sec. 3. In Sec. 4 we discuss the angular momentum evolution and distribution for the different models,and we discuss the influence of the early outflows in Sec. 5. Finally, we conclude the results of this work in Sec. 6.

2. Numerical modeling

For this study we follow the collapse of Bonnor-Ebert-type (Ebert 1955; Bonnor 1956) molecular cloud cores using the AMR based FLASH code (Fryxell et al. 2000) to solve the gravito-magneto-hydrodynamic equations (details on the Bonnor-Ebert-Profile and of this setup can be found in Banerjee et al. (2004), henceforth BPH04). We study the collapse of three different cases which all have the same initial density and temperature distribution. The three cases are:

- The isothermal case (iso): Here, we assume an isothermal equation of state (adiabatic index, $\gamma = 1.0001$) throughout the calculation.
- The hydro case (hydro): For this case we incorporate the cooling ability from molecular and dust radiation in the optical thin regime and use a radiation diffusion approxima-

tion in the optical thick regime. Details of our cooling treatment can be found in the appendix of BPA06.

- The magnetized case (mag): Here, we apply an initial magnetic field parallel to the rotation axis (z-axis) and use the same cooling as in the pure hydro case.

The three different cases presented in this study, have the same initial values for the total mass of the cloud core, $M = 168\,M_\odot$, its radius, $R = 3.34 \times 10^5\,\mathrm{AU} = 5 \times 10^{18}\,\mathrm{cm}$, and the BE-core density, $\rho_0 = 3.35 \times 10^{-21}\mathrm{g\,cm^{-3}}$. We also enhance the density of all cores by 10% and add a 10% $m = 2$ density perturbation. The initial free fall time associated with the core region is $t_{\rm ff} = \sqrt{3\pi/32\,G\,\rho_0} = 3.63 \times 10^{13}$ sec $= 1.1 \times 10^6\,\mathrm{yrs}$. We also give the cloud cores a slight spin with a constant angular velocity. The two non-magnetic simulations start with an angular velocity of $\Omega = 5.5 \times 10^{-15}\,\mathrm{rad\ sec^{-1}}$ whereas the magnetized case rotates with an angular velocity of $\Omega = 1.1 \times 10^{-14}\,\mathrm{rad\ sec^{-1}}$. We increase the initial rotation by a factor of two in the magnetized case because magnetic braking spins down the sphere substantially prior to the collapse (see Banerjee & Pudritz 2006). These initial conditions are equivalent to an $\Omega\,t_{\rm ff}$ of 0.2 and 0.4 for the non-magnetized and magnetized cases, respectively. In BPH04 we showed that the former case results in a ring which fragments into a binary system if only molecular cooling is considered. The initial isothermal sound speed, $c_{\rm iso}$, is in all cases $0.408\,\mathrm{km\ sec^{-1}}$.

Initially, the magnetic field in the magnetized case is given only a component parallel to the rotation axis (z-axis) where B_z varies between $0.33\,\mu$G and $1.36\,\mu$G corresponding to a constant $\beta \equiv p/(B^2/8\pi) = 76$ in the equatorial plane. This gives a mass-to-flux ratio of $M/\Phi_B = 3.2/\sqrt{G}$ which is highly supercritial (the critial value is $\sim 0.12/\sqrt{G}$). Nevertheless the magnetic field becomes dynamically important during the collapse and will be able to drive outflows and jets as we will see later. This choice of a supercritical core is in agreement with recent work by Tilley & Pudritz (2005) which studied the formation of turbulent fragmentation and the IMF in magnetized turbulent clumps. In that paper, it was demonstrated that substantially supercritical clumps did a far better job in reproducing the observations of the core mass function in cluster forming environments, than did clumps that were nearer to magnetically critical values. One way that this can easily occur in a turbulent environment is for shocks to rapidly assemble cores by flows along field lines.

The choice of our initial core mass is taken from recent observations of cores in regions of high mass star formation (e.g., Reid & Wilson 2006). The actual physical values we use arise in this context arise from the consideration of a BE sphere with a core density of $10^3\,\mathrm{cm^{-3}}$ ($3.35 \times 10^{-21}\,\mathrm{g\,cm^{-3}}$) at $20\,K$ which is a typical value of such molecular cores. As we will see later, the mass accretion rate depends only weakly on the initial mass of the core.

3. High accretion rates during the collapse phase

The collapse of spherical cloud cores has been studied by many authors, both analytically and numerically (see e.g., Larson 1969; Penston 1969; Shu 1977; Hunter 1977; Whitworth & Summers 1985; Foster & Chevalier 1993; Hennebelle et al. 2003; Banerjee et al. 2004). In the case of an initial singular isothermal sphere (SIS) there exists an elegant self-similar solution to this problem wherein an expansion wave travels from the (singular) center outward with the speed of sound, thereby initiating an inside-out collapse (Shu 1977). However, as pointed out by Whitworth et al. (1996) a SIS configuration is unnatural because – among other difficulties – its collapse can not produce binaries (see also Pringle 1989). The collapse of non-singular (ie Bonner -Ebert) cores proceed differently than singular spheres and have distinguishable implications. Firstly – as demonstrated by many authors (e.g., Larson 1969; Penston 1969; Foster & Chevalier 1993; Hennebelle et al. 2003; Banerjee et al. 2004) – the collapse proceeds from the *outside-in* rather than from the inside-out and the density maintains a flat profile at the core center, where the core size is of the order of the local Jeans length at every epoch (see also Whitworth & Summers 1985, for a summary of analytic solutions). Secondly, the radial distribution of the infall velocity peaks at the edge of the flat density core and falls off quickly towards the center (e.g. see Fig. 3 in BPH04). The velocity also becomes supersonic as the core density increases and the size of the flat region shrinks. Recent observations of a pre-Class 0 object show that the collapse proceeds supersonically, strongly supporting a Larson-Penston-type collapse rather than an expansion wave-type collapse (Furuya et al. 2006). Thirdly – and of great importance – the mass accretion in the non-selfsimilar case is much higher than predicted from the selfsimilar collapse of a singular isothermal sphere. We find that the mass accretion in the early phase of the collapse is

$$\dot{M} \approx 20 - 100\,\frac{c^3}{G} \tag{1}$$

(c is the isothermal sound speed and G is Newton's gravitational constant). Note the self-similar SIS collapse gives a mass accretion of only $0.96\,c^3/G$. Typical values of the sound speed in cold cloud cores ($T \sim 20\,\mathrm{K}$) are of the order of a few $10^2\,\mathrm{m\,sec^{-1}}$ which gives $c^3/G \sim 10^{-6} - 10^{-5} M_\odot\,\mathrm{yr}^{-1}$. Our result from numerical simulations are in agreement with the early analytic results of Larson (1969) and Penston (1969) (see also Hunter 1977; Whitworth & Summers 1985).

The remarkable point of this result is that the high accretion rates are achieved even without initial turbulence and during the isothermal phase of the collapse. The main reason for the high accretion rate in this idealized case is the supersonic infall velocity, v_r, close to the peak density. Even moderate Mach numbers, $\mathcal{M}$, of $2-3$ (The Larson asymptotic Mach

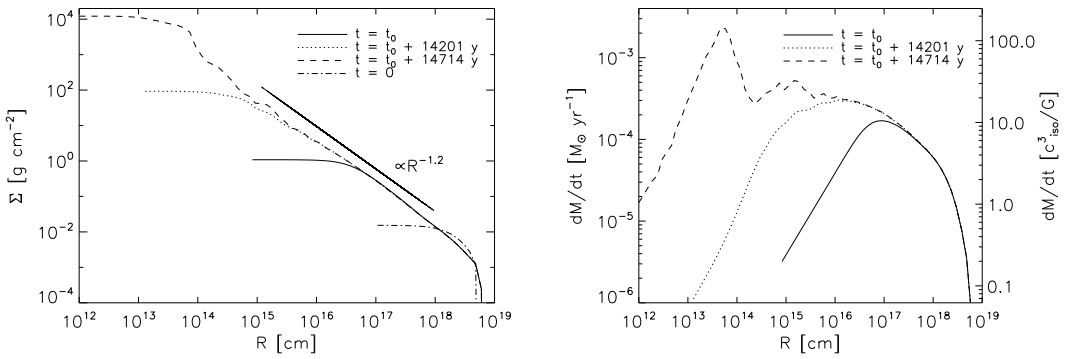

Fig. 1.— Shows the time evolution of the column density and mass accretion in the magnetized case. We assume the beginning of the collapsing phase at $t = t_0$ when the column density reaches $\Sigma_{\rm core} \approx 1\,{\rm g\,cm^{-2}}$ and the pressure is $P/k_B \approx 10^8\,{\rm K\,cm^{-3}}$ (see Fig. 2). At $t = t_0$ the mass density in the core is $\rho_{\rm core} = 2.44 \times 10^{-17}\,{\rm g\,cm^{-3}}$ corresponding to a free fall time of $t_{\rm ff} = 1.35 \times 10^4\,{\rm yrs}$. At $t = t_0 + 1.1\,t_{\rm ff}$ the core density reached already $10^4\,{\rm g\,cm^{-2}}$. The initial profile of our simulation is marked by $t = 0$.

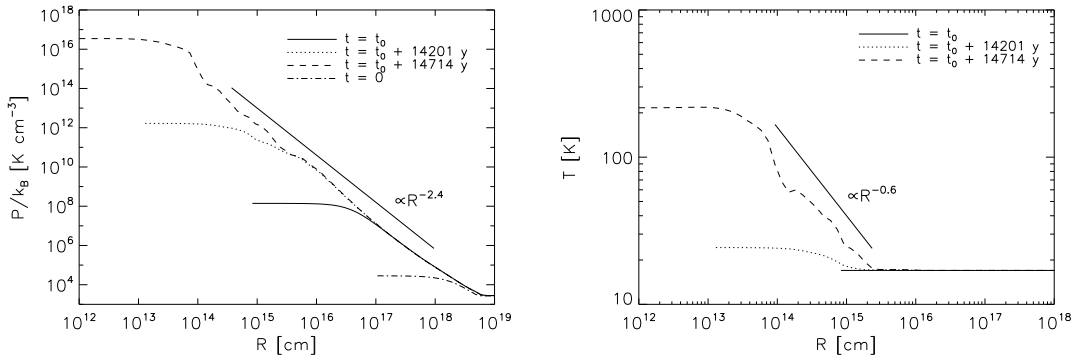

Fig. 2.— Shows the time evolution of the pressure and temperature in the magnetized case. See Fig. 1 for the corresponding column densities and label explanations. The pressure scales as $P \propto \Sigma^2$ and the temperature develops a $R^{-0.6}$ profile within the warm, dense region.

number is $\mathcal{M} \sim 3$) enhances the mass accretion rates relative to c^3/G because

$$c^3/G \rightarrow v_r^3/G = \mathcal{M}^3\, c^3/G \tag{2}$$

in the supersonic limit. Additionally, the core is continually embedded in a high pressure environment.

One-dimensional numerical studies of the long term evolution (i.e. beyond one dynamical time) of a collapsing BE-Sphere by Foster & Chevalier (1993) showed that the mass accretion is not constant but decreases with time after reaching a peak value. Beyond this peak, the remaining gas in the envelope drains out with an ever smaller accretion rate over time. This situation could be different for the collapse of realistic cloud cores, which are certainly not isolated objects but are instead surrounded by a clumpy media and attached to filaments wherein accretion might sustain high rates for a longer time.

Using the magnetized simulation as the fiducial case, we show the evolution of the column density and corresponding mass accretion rates in Fig. 1 and in Fig. 2 the evolution of the pressure and temperature as functions of the disk radius [1]. When the density approaches $\Sigma \sim 1\,\mathrm{g\,cm^{-2}}$ (we denote the corresponding time as t_0) the mass accretion rate is already $\sim 10^{-4}\,M_\odot\,\mathrm{yr^{-1}}$ and the surrounding pressure is $10^8\,\mathrm{K\,cm^{-3}}\,k_B$. These results are in agreement with the model of McKee & Tan (2002, 2003) who showed that this high pressurized, compact cloud cores accrete gas with accretion rates as high as $10^{-3}\,M_\odot\,\mathrm{yr^{-1}}$. We find that accretion rates of this order ($\sim 10^{-3}\,M_\odot\,\mathrm{yr^{-1}}$) are reached within only $\sim 14.7 \times 10^3\,\mathrm{yrs}$ which corresponds to 1.1 dynamical times. The core column density after one dynamical time is $\sim 10^4\,\mathrm{g\,cm^{-2}}$ while the pressure achieves a value $P/k_B \approx 3.5 \times 10^{16}\,\mathrm{K\,cm^{-3}}$. As long as the core remains isothermal (the most efficient cooling regime), the pressure scales with the column density as $P \propto \Sigma^2$ (i.e. the pressure profile is close to $R^{-2.4}$) and slightly steeper in the inefficient cooling regime where the temperature rises during the collapse (see right panel of Fig. 2). The continuously high external pressure and the supersonic infall velocity maintains the high mass accretion. We also show the mass accretion scaled to the quantity c_{iso}^3/G (c_{iso} is the *initial* isothermal sound speed) in Fig. 1. From this one can see that accretion is much more efficient (by a factor of ~ 100) than expected from the collapse of a SIS.

These results show that high mass accretion rates are a natural result of the early collapse phase of (non-singular) collapsing cloud cores with flat-topped density profiles. Turbulent driving for the rapid assembly of massive stars is not a necessary ingredient, although it does further enhance the accretion rate as shown in analytic models (McKee & Tan 2002, 2003).

---

[1] All quantities which are functions of the disk radius, R, are azimuthally averaged and density weighted, e.g. $f(R) = (2\pi\,\Sigma(R))^{-1} \int \mathrm{d}z\,\mathrm{d}\phi\,\rho(\mathbf{x})\,f(\mathbf{x})$, where $\Sigma(R) = (2\pi)^{-1} \int \mathrm{d}\phi\,\mathrm{d}z\,\rho(\mathbf{x})$ is the column density.

The enhancement is even larger in fully realized 3D turbulence, due to filamentary accretion (see e.g., BPA06).

For comparison, we summarize the collapse phase of the three different cases (mag, hydro, iso) in the Figs. 3 – 5 at the time when the column density reaches $5 \times 10^3\,\mathrm{g\,cm^{-2}}$. Common features can be seen mainly in the envelope of the collapsing cores. All three cases end up with a column density profile which is close to $\propto R^{-1.2}$ in the disk envelope (see left panel of Fig. 3). In the inner part of the disk ($\lesssim 100\,\mathrm{AU}$) the influence of the (inefficient) cooling processes and magnetic fields become visible. The non-isothermal cases develop a steeper density profile as infalling material tends to pile up at the shock regions at the edge of the warm core. These shock regions appear at a radial distance of $\sim 20\,\mathrm{AU}$ because the core becomes opaque inside this radius (BPA06). The difference with the isothermal case inside $\lesssim 100\,\mathrm{AU}$ can also be seen in the mass distribution of the disk which we show in the right panel of Fig. 3. More material accumulates in the hydro and magnetized cases at the time when all three cases reached a peak column density of $5 \times 10^3\,\mathrm{g\,cm^{-2}}$.

We show the comparison of the mass accretion rates of the three different cases in Fig. 4. The right panel gives the mass accretion in terms of solar masses per year and compared to the initial isothermal sound speed, whereas the right panel shows this value scaled to the local sound speed quantity $c^3_{\rm local}/G$. In physical terms (i.e. $M_\odot/\mathrm{yr}$) the hydro case is most advanced and accretes gas with several $10^{-3}\,M_\odot\,\mathrm{yr}^{-1}$ corresponding to $\sim 300\,c^3_{\rm iso}/G$. Then again, the accretion rates of all three cases are very similar when compared to local quantity $c^3_{\rm local}/G$ ($\sim 40\,c^3_{\rm local}/G$). This shows, again, that the estimate for the mass accretion in the supersonic regime is sensitive to the Mach number and the local sound speed. To complete this picture, we show the infall velocity in Fig. 5 measured in km/ sec and $c_{\rm iso}$ (left panel) and in terms of the local sound speed (right panel). The high infall velocity (and therefore the high mass accretion) in the hydro case is due to the warm core region which has a high sound speed. The local Mach number of all three cases differs only within a range $2 - 2.5$ whereas the isothermal Mach number ranges from $2.5 - 4$ between them.

We also point out that the mass accretion during this early stage of collapse does not strongly depend on the initial mass of the cloud core (the good estimate of Eq. 2 does not have a mass dependence). In BPH04 and Banerjee & Pudritz (2006) we showed that a $\sim 2M_\odot$ cloud core reaches also mass accretion rates of $10^{-4} - 10^{-3} M_\odot/\mathrm{yr}$.

In summary, we find that the typical infall velocity of a collapsing cloud core is $2-3\,c_{\rm local}$ which recovers earlier results studying the isothermal collapse phase (e.g., Larson 1969; Foster & Chevalier 1993). The supersonic infall velocity is the main reason for the high mass accretion of collapsing cloud cores. Furthermore, the increased local sound speed due to thermal effects in the warm core region enhances the mass accretion in the post-isothermal

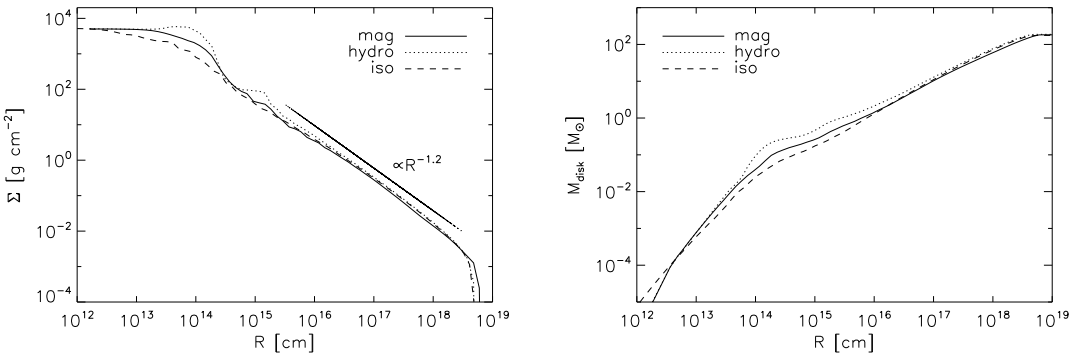

Fig. 3.— Comparison of the column density profiles and disk masses for three different cases, hydromagnetic (mag), pure hydro (hydro), and pure isothermal (iso) simulation at the time when they reached the same core column density $\Sigma_{\rm core} \sim 5 \times 10^3\,{\rm g\,cm^{-2}}$.

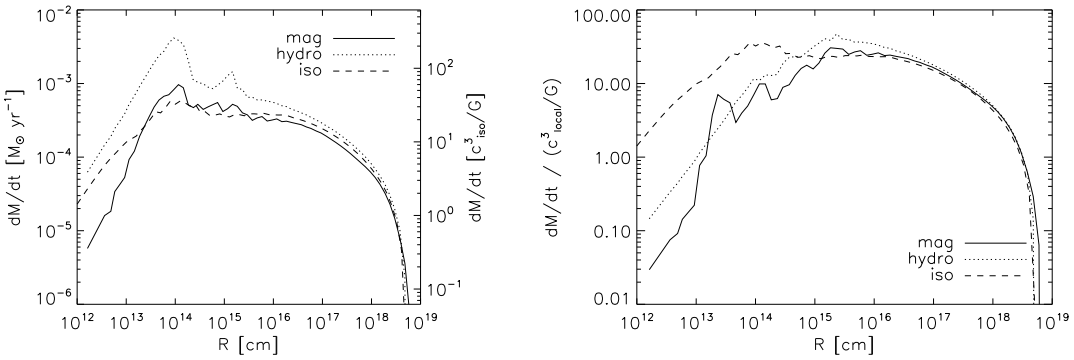

Fig. 4.— Comparison of the mass accretion rate for the three different cases, hydromagnetic (mag), pure hydro (hydro), and pure isothermal (iso) simulation at the time they reached the same core density (see Fig. 3). The left panel shows the mass accretion in units of $M_\odot\,{\rm yr}^{-1}$ whereas the right panel shows the same quantity compared to $c^3_{\rm local}/G$, where $c_{\rm local}$ is *local* sound speed.

regime.

4. Angular momentum extraction by bars and magnetic fields

Most stars, if not all, rotate. The origin of stellar angular momentum is in itself an important problem in star formation theory. It has a natural explanation in the turbulent fragmentation picture, where it arises from the oblique shocks that create the dense cores (eg. Tilley & Pudritz 2004). Strict conservation of the specific angular momentum in a core would inhibits accretion through the protostellar disk whenever the infalling gas hits its centrifugal barrier. The issue of redistributing or extracting the angular momentum within the protostellar disk is important for understanding the assembly of (massive) stars.

In Fig. 6 we show the evolution of the specific angular momentum in the magnetized case as a function of radius (left panel) and enclosed mass in the disk (right panel). Infalling, high angular momentum gas increases the specific angular momentum at small radial distances with time. Apart from the advection of angular momenta due to the accreting gas, there is additionally, a resorting of disk angular momentum operating due to turbulence. This can be seen from the right panel of Fig. 6 where we plot the specific angular momentum as a function of the enclosed mass. This is a useful thing to do because this quantity is constant with time if angular momentum is *not* redistributed within the disk (see e.g., Abel et al. 2002). For the magnetic case shown in Fig. 6 the angular momentum is *decreasing* with time within the disk (inside $M_{\rm disk} \lesssim 1\,M_\odot$). This decrease of angular momentum at a given mass shell allows for continuing efficient accretion through the disk plane. In particular, we find that the specific angular momentum changes by an amount of $\Delta j_z \sim 5.3 \times 10^{19}\,{\rm cm}^2\ {\rm sec}^{-1}$ (i.e. by a factor of 2.8) at a mass shell of $0.1\,M_\odot$ within $14.7 \times 10^3\,{\rm yrs}$. In the magnetized case the angular momentum is extracted by magnetic braking, magnetic torque, the launching of an outflow, and by the development of a bar in the disk. Depending on the field geometry and strength magnetic braking by a poloidally dominated magnetic field can be an efficient way to extract angular momentum (Mouschovias & Paleologou 1979, 1980). An additional toroidal component of the magnetic field gives rise to a magnetic torque (e.g., Konigl & Pudritz 2000) which in the case of rotationally generated toroidal field (backwards bend field) extracts angular momentum from the protodisk. In Banerjee & Pudritz (2006) we showed that the magnetic torque can be a substantial fraction (10% – 50%) of the angular momentum flux from the accreting gas.

In Fig. 7 we compare the angular momentum distribution and the rotational velocity for the three different cases (Note that the overall enhancement of the angular momentum and rotational velocity in the magnetized case is due to the initially higher angular velocity).

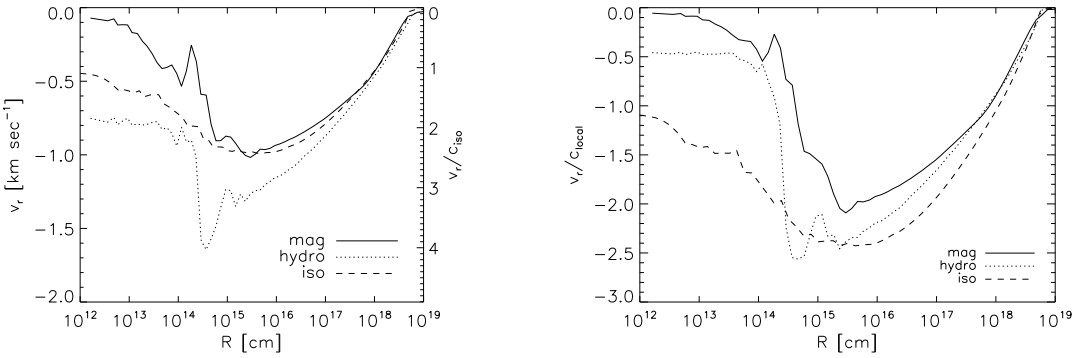

Fig. 5.— Comparison of the radial infall velocity for the three different cases, hydromagnetic (mag), pure hydro (hydro), and pure isothermal (iso) simulation at the time they reached the same core density (see Fig. 3). The left panel shows the infall velocity in km/sec and compared to the initial isothermal sound speed, $c_{\rm iso}$, and the right panel shows the same quantity measured with the *local* sound speed, $c_{\rm local}$.

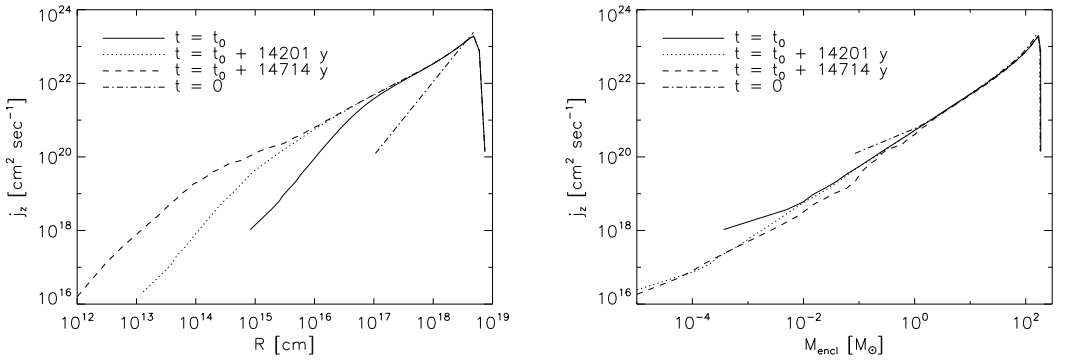

Fig. 6.— Shows the time evolution specific angular momentum as a function of radius and enclosed mass in the magnetized case. See Fig. 1 for the corresponding column densities and label explanations.

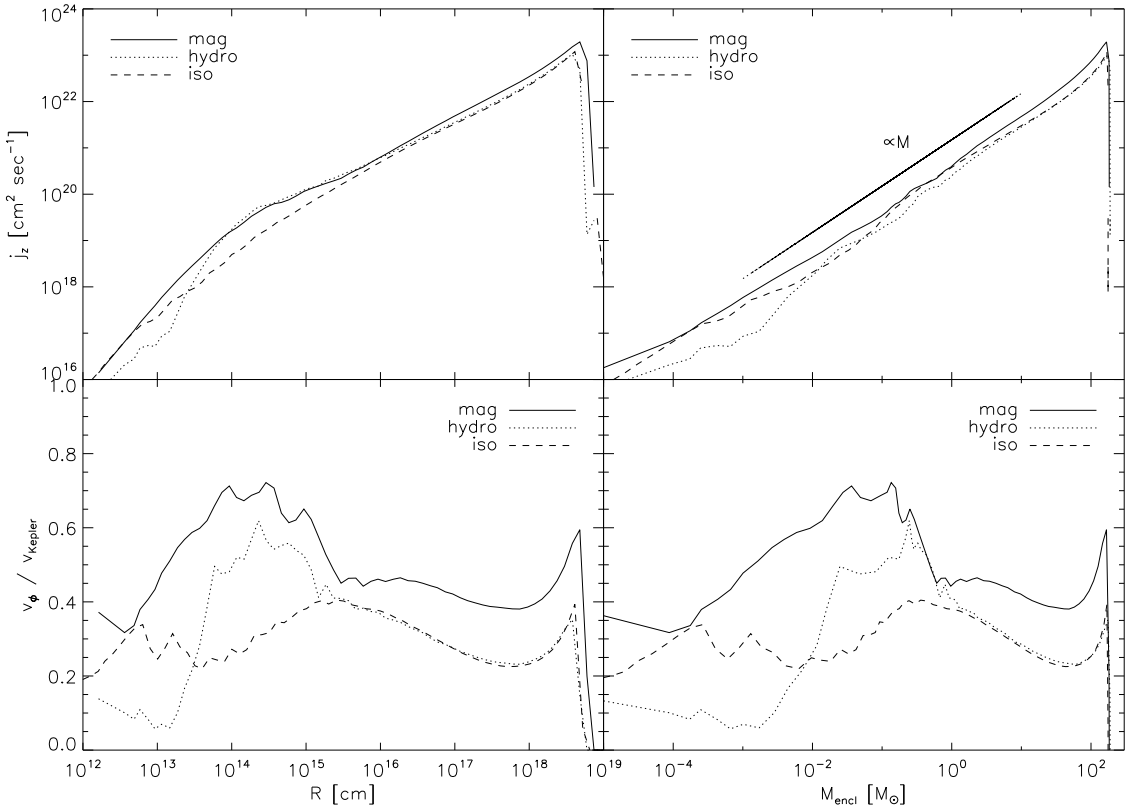

Fig. 7.— Comparison of the specific angular momenta and rotational velocity for the three different cases, hydromagnetic (mag), pure hydro (hydro), and pure isothermal (iso) simulation at the time they reached the same core density of $5 \times 10^3\,\mathrm{g\,cm^{-2}}$ (see Fig. 3). The left panels show this quantities as a function of the radial distance and the right panels show the same quantities as functions of the enclosed disk mass, $M_{\rm encl}$. Note that the initial rotation in the magnetic case is two time larger than in the two other cases (see also Sec. 2)

During this early stage of the collapse, the disk is still more massive than the central object(s) and is still out of equilibrium. In all three cases the rotational velocity is sub-Keplerian with 10% to 60% of the centrifugal velocity. Apart from the general common features of the angular momentum distribution of the three models there are important differences. Both of the non-isothermal cases show a 'pile-up' of high angular momentum gas at the shock fronts which sets the edge of the disk. This can be seen in the lower left panel of Fig. 7 where the high rotational velocity material accumulates at the shock distance of few $\times$ 10 AU. Inside the protodisk (inside the shock fronts) the angular momentum is very efficiently transported by the large bars and/or the magnetic field (see Figs. 8 and 9). Therefore, the rotational velocity drops rapidly towards smaller radii in the hydro and magnetized case. The isothermal case shows a much more evenly distributed toroidal velocity when compared to the Keplerian velocity. The reason here is the absence of shocks in the disk plane which allows a continuous inflow of high angular momentum gas. Additionally, the absence of a strong bar in the isothermal case does not allow for efficient transport of angular momentum (see Fig. 10).

We investigate this further by presenting 2D snapshots of the disk planes for the three different cases in Figs. 8 – 10 on a scale of $\sim$ 300 AU and $\sim$ 40 AU, respectively. Both the magnetized (Fig. 8) and the hydro simulation (Fig. 9) developed a large bar with an extent of $\sim$ 250 AU. Comparing the small scale structure of the magnetized and hydro case (right panel of Figs. 8 and 9) one sees that the former case develops a larger, more rotationally supported protodisk. This is due to the additional magnetic pressure and the higher toroidal velocity in the magnetized case. Both cases accrete efficiently gas through their bars/spiral arms onto the protodisk. This can be seen particularly well in the right panel of Fig. 9 where high density gas is streaming along the spiral arms towards the central object. The isothermal case also developed a bar but it is much smaller and less pronounced. Therefore, the drop of the rotational velocity (measured in Keplerian velocity) towards the disk center is only a factor of two (in the hydro case the rotational velocity decreases by a factor of 6).

5. Early outflows during massive star formation

Little is known observationally about the influence of outflows on the early assembly of massive stars. On one hand, they could reduce the mass accretion onto the massive (proto)star if the outflow carries a substantial mass. On the other, early outflows provide a natural anisotropy of the accreting gas which results into low density cavities. Such cavities are like funnels out of which the radiation from the already active star can escape. Without such a pressure-release valve, trapped radiative flux would halt the in-fall. Krumholz et al.

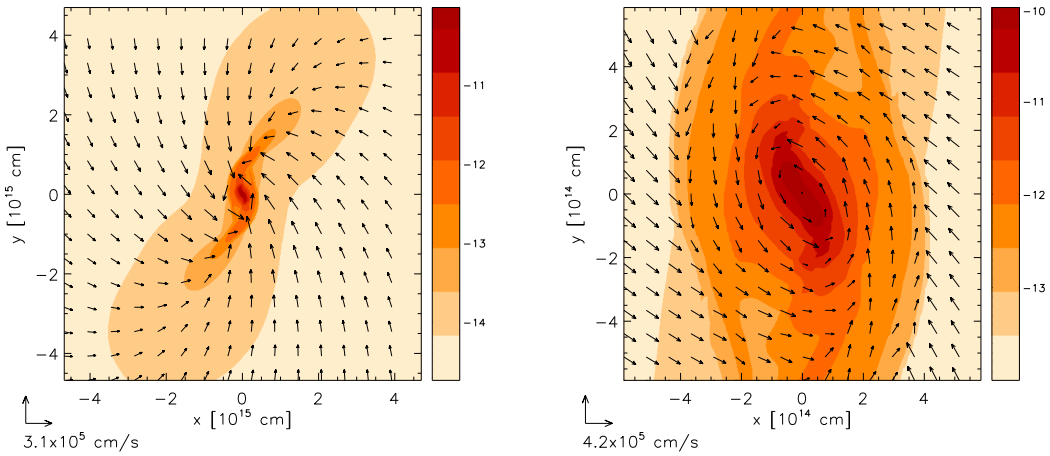

Fig. 8.— Magnetized case: The panels show 2D slices through the disk plane at two different scales (large scales at right and small scales at the left). This snapshot is taken 1.4×10^4 yrs into the collapse, corresponding to $\Sigma_{\rm core} \approx 5 \times 10^3\,{\rm g\,cm^{-2}}$ (see Fig. 3).

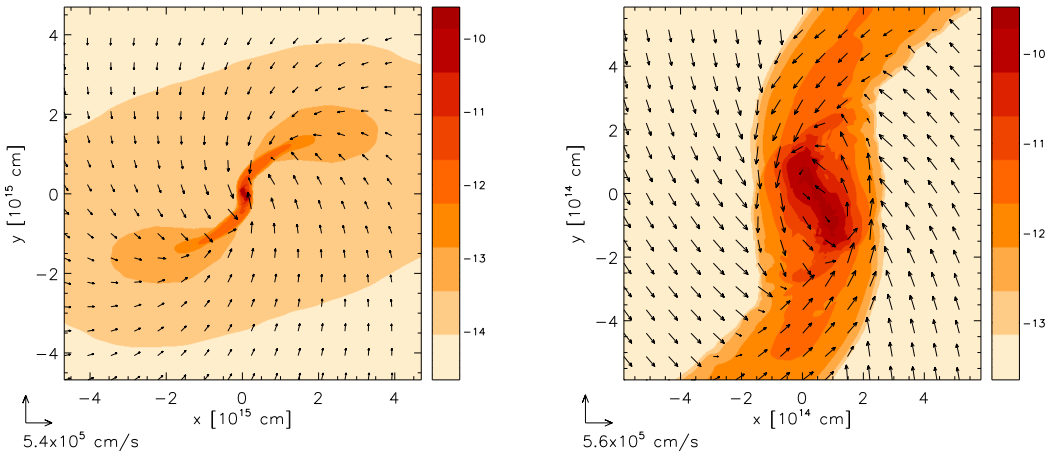

Fig. 9.— The hydro case: the panels show 2D slices in the disk plane at two different scales (large scales at right and small scales at the left). This snapshot is taken 1.4×10^4 yrs into the collapse, corresponding to $\Sigma_{\rm core} \approx 5 \times 10^3\,{\rm g\,cm^{-2}}$ (see Fig. 3).

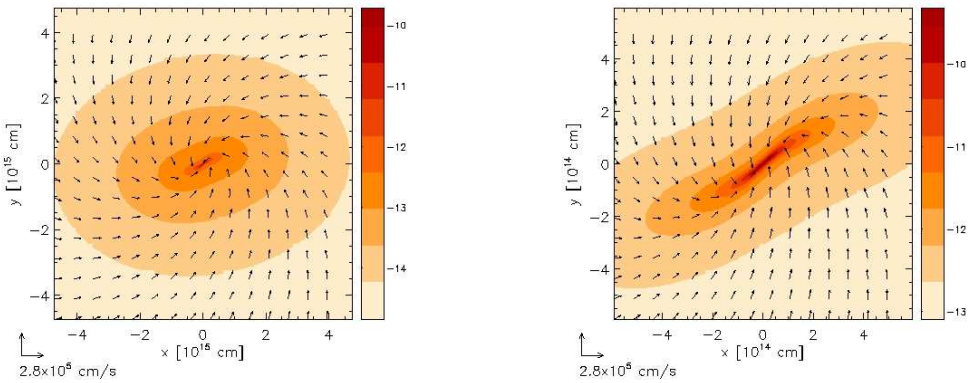

Fig. 10.— The isothermal case: the panels show 2D slices in the disk plane at two different scales (large scales at right and small scales at the left). This snapshot is taken 10^4 yrs into the collapse, corresponding to $\Sigma_{\rm core} \approx 5 \times 10^3\,{\rm g\,cm^{-2}}$ (see Fig. 3).

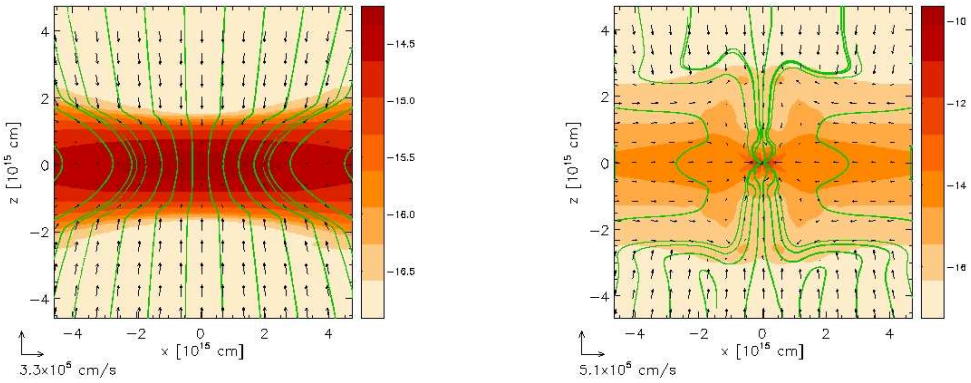

Fig. 11.— Shows 2D snapshots perpendicular to the disk plane of the magnetized case at different times on large scales ($\sim 300\,{\rm AU}$). The left panel shows the situation at $t = t_0 + 1.31 \times 10^4\,{\rm yrs}$ ($0.98\,t_{\rm ff}$) into the collapse and the right panel shows the configuration 1566 yrs later after magnetic pressure inflates the disk and the outflow is launched (see also Fig. 12 for a close-up).

(2005) studied the effect of outflow-funnels using a Monte Carlo radiative-transfer method which shows that radiation pressure is greatly reduced by radiation escaping through the outflow cavities.

Magnetic fields coupled to the protostellar disk can be the driving power for such outflows. A variety of self-consistent simulations of collapsing magnetized cloud cores show that outflows are launched if the toroidal magnetic field pressure overcomes the gravitational force (Tomisaka 1998, 2002; Matsumoto & Tomisaka 2004; Machida et al. 2004; Banerjee & Pudritz 2006). This early-type outflows can be understood in terms of a growing magnetic tower (Lynden-Bell 2003): The rotating (proto)disk generates a strong toroidal field component by winding up the threading field lines. The resulting magnetic pressure is in local equilibrium with the gravitational force and the ram pressure of the infalling material. But every further rotation increases the toroidal field component thereby shifting the equilibrium location (which is characterized by a shock) towards higher latitudes. The result is an inflating magnetic bubble in which material is lifted off the disk.

Some of the highlights of this paper are shown in the following figures, wherein we explicitly demonstrate the launch of the outflow. We present 2D cuts through our 3D data, which are shown as the images in Figs. 11 and 12. These show the collapse state at different times and physical scales. The time sequence shown in Fig. 11 demonstrates the situation shortly before the launching of the outflow (left panel) and roughly 1600 yrs later (right panel). On this large scales ($\sim 300\,\mathrm{AU}$) one can see the strong bending of the dragged-in magnetic field lines (the toroidal component is not shown in the 2D slices) and the inflated protodisk. Also clearly visible are the shock fronts which separate the disk from the accreting environment.

Close-ups ($\sim 20\,\mathrm{AU}$) of the early stage of the outflow launching are shown in Fig. 12, where we zoom in by a factor of 10 in comparison with the previous figures. Here again the collapsing stage shortly before the flow reversal is shown in the left panel and the onset of the outflow (less than 200 yrs later) is shown in the right panel. Due to the stronger magnetic field strength deeper in the gravitational potential well, the outflow velocity ($\sim 4\,\mathrm{km\ sec^{-1}}$) is higher than on larger scales which powers a stronger outflow.

It is also worth emphasizing that outflow only occurs when magnetic fields are included in the simulations. In this paper (as in our others), we have never seen outflows associated with our purely hydrodynamic collapses. We conclude that purely hydrodynamic collapse misses a critical ingredient in stellar formation - namely- the early launch of disk related outflows.

6. Summary and Conclusions

In this work we simulated the 3D collapse of magnetized, massive molecular cloud cores which are the progenitors of massive stars. We carried out this investigation at early stages of the collapse, long before a massive star has even assembled at the center of the resulting disk. Using three different 3D collapse simulations (an isothermal case, a pure hydro case with radiative cooling, and a magnetized case) of Bonnor-Ebert type cloud cores we show that the mass accretion during the collapse phase is much more efficient than calculated from the collapse of a singular isothermal sphere (SIS).

We find that the mass accretion rates can reach $\sim 10^2\, c^3/G$ which is a factor of 10^2 higher than the SIS case. This high mass accretion is due to the supersonic infall velocity and the high pressure at the edge of the collapsing core, where the pressure increases with density as $P \propto \Sigma^2$. The mass accretion can be estimated by $\dot{M} \sim v_r^3/G = \mathcal{M}^3\, c^3/G$ where the Mach number, $\mathcal{M}$, can reach 3 or more with infall velocities ranging from $1 - 1.5\,\mathrm{km\ sec^{-1}}$. Note that, due to inefficient cooling at densities of $\Sigma \gtrsim 10\,\mathrm{g\,cm^{-2}}$ the temperature and therefore the sound speed increases which in turn results in a higher physical mass accretion rates. Therefore, mass accretion rates of $10^{-3}\, M_\odot\,\mathrm{yr^{-1}}$ and higher are easily reached in the early stage of the assembly of massive stars. This high accretion rates allow the formation of massive stars in only $10^4\,\mathrm{yrs}$. A formation time scale of only $10^4\,\mathrm{yrs}$ is short enough for the massive star to build up before its surrounding disk is photo-evaporated from the UV environment emitted from the surrounding OB association (Hollenbach et al. 2000; Richling & Yorke 1998). This allows also for an unified picture of star formation where low *and* high mass star form the same way from the collapse of an overdense cloud core. This unified theory is strongly supported by recent observations of the assembly of massive stars through accretion disks (Chini et al. 2004, 2006) and from the detection of high accretion rates onto a very young massive star (Beltrán et al. 2006).

Furthermore, we find that angular momentum is efficiently transfered by bars/spiral arm and magnetic torque. The simulations with radiative processes develop a larger bar-like structure than the isothermal case and are less rotationally supported in the inner region of the disk. The reduced specific angular momenta also enhance the accretion rate as low angular momentum gas can be accreted more efficiently. In particular we showed that the specific angular momentum decreases by a factor of 2.8 within $14.7 \times 10^3\,\mathrm{yrs}$ ($1.1\, t_{\rm ff}$) into the collapse. In all cases, an equilibrium disk did not yet develop because at this early stage, the disk is still much more massive than the central object. At this stage the rotational velocities are sub-Keplerian and and range from $0.4 - 0.7\, v_{\rm Kep}$ within the protodisk.

Outflows play an important role in this process by reducing the radiation pressure which can escape through funnels carved by the expelled gas (Krumholz et al. 2005). Here, we have

shown that that outflows are a natural consequence of the early stages of collapsing, massive magnetized (and not purely hydrodynamic) cloud cores. This process is not restricted just to the case of low mass star formation which we previously examined. Recent observations indicate also early type outflows (e.g., Shepherd 2003) which might be associated with magnetic fields.

The critical issue that we have uncovered is that for both low (our previous work) and high mass star formation (this work), magnetic pressure from a wound-up toroidal field becomes eventually strong enough to reverse the infalling gas and launch an outflow. We find that the outflow has the shape of a hollow cylinder which outflow speed reaches up to $5\,\mathrm{km\ sec^{-1}}$ at 20 AU above and below the disk midplane (see e.g. Banerjee & Pudritz 2006, on details on magnetically driven outflows).

We conclude that this universality in the formation of disks and the early formation of outflow cavities that are created by the jets that are launched from their surfaces, implies that the radiation pressure from massive stars appears too late on the scene to substantially affect the assembly of a massive star by disk accretion. We are pursuing more detailed computations of this picture that will eventually include radiative feedback within more complex, cluster forming environments.

We thank the anonymous referee for some useful remarks. The FLASH code was developed in part by the DOE-supported Alliances Center for Astrophysical Thermonuclear Flashes (ASC) at the University of Chicago. Our simulations were carried out on computer clusters of the SHARCNET HPC Consortium. REP is supported by the Natural Sciences and Engineering Research Council of Canada.

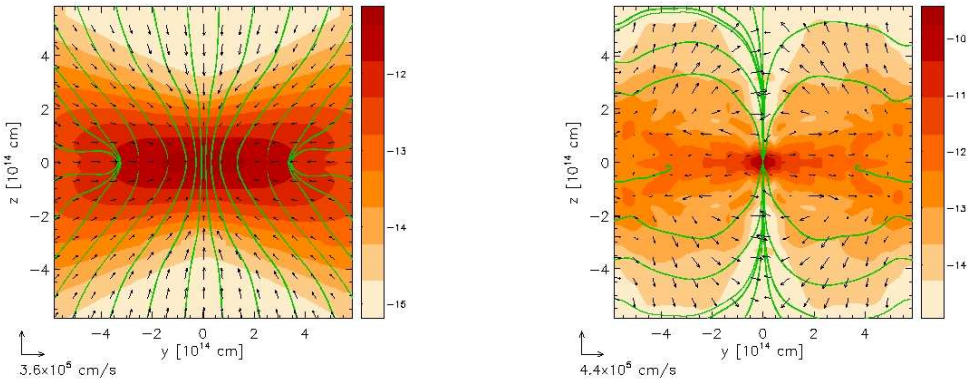

Fig. 12.— Close-up 2D snapshots of the disk region (perpendicular to the disk in the yz-plane) in the magnetized case. The left panel shows the situation at $t = 1.45\times10^4$ yrs ($1.08\,t_{\rm ff}$) into the collapse and before the flow reversal and right panel shows the configuration 188 yrs later when the outflow is clearly visible.

REFERENCES

Abel, T., Bryan, G. L., & Norman, M. L. 2002, Science, 295, 93

Banerjee, R., & Pudritz, R. E. 2006, ApJ, 641, 949

Banerjee, R., Pudritz, R. E., & Anderson, D. 2006, MNRAS in print, e-print: astro-ph/0609428

Banerjee, R., Pudritz, R. E., & Holmes, L. 2004, MNRAS, 355, 248

Beltrán, M. T., Cesaroni, R., Codella, C., Testi, L., Furuya, R. S., & Olmi, L. 2006, Nature, 443, 427

Bonnell, I. A., Bate, M. R., & Zinnecker, H. 1998, MNRAS, 298, 93

Bonnor, W. B. 1956, MNRAS, 116, 351

Chini, R., Hoffmeister, V., Kimeswenger, S., Nielbock, M., Nürnberger, D., Schmidtobreick, L., & Sterzik, M. 2004, Nature, 429, 155

Chini, R., Hoffmeister, V. H., Nielbock, M., Scheyda, C. M., Steinacker, J., Siebenmorgen, R., & Nürnberger, D. 2006, ApJ, 645, L61

Ebert, R. 1955, ZAp, 37, 217

Foster, P. N., & Chevalier, R. A. 1993, ApJ, 416, 303

Fryxell, B., Olson, K., Ricker, P., Timmes, F. X., Zingale, M., Lamb, D. Q., MacNeice, P., Rosner, R., Truran, J. W., & Tufo, H. 2000, ApJS, 131, 273

Furuya, R. S., Kitamura, Y., & Shinnaga, H. 2006, accepted by ApJ preprint doi:10.1086/'508405, e-print: astro-ph/0608357

Hennebelle, P., Whitworth, A. P., Gladwin, P. P., & André, P. 2003, MNRAS, 340, 870

Hollenbach, D. J., Yorke, H. W., & Johnstone, D. 2000, Protostars and Planets IV, 401

Hunter, C. 1977, ApJ, 218, 834

Kahn, F. D. 1974, A&A, 37, 149

Konigl, A., & Pudritz, R. E. 2000, Protostars and Planets IV, 759

Krumholz, M. R., McKee, C. F., & Klein, R. I. 2005, ApJ, 618, L33

Larson, R. B. 1969, MNRAS, 145, 271

Lynden-Bell, D. 2003, MNRAS, 341, 1360

Machida, M. N., Tomisaka, K., & Matsumoto, T. 2004, MNRAS, 348, L1

Matsumoto, T., & Tomisaka, K. 2004, ApJ, 616, 266

McKee, C. F., & Tan, J. C. 2002, Nature, 416, 59

—. 2003, ApJ, 585, 850

Mouschovias, T. C., & Paleologou, E. V. 1979, ApJ, 230, 204

—. 1980, ApJ, 237, 877

Patel, N. A., Curiel, S., Sridharan, T. K., Zhang, Q., Hunter, T. R., Ho, P. T. P., Torrelles, J. M., Moran, J. M., Gómez, J. F., & Anglada, G. 2005, Nature, 437, 109

Penston, M. V. 1969, MNRAS, 145, 457

Pringle, J. E. 1989, MNRAS, 239, 361

Reid, M. A., & Wilson, C. D. 2006, ApJ, 644, 990

Richling, S., & Yorke, H. W. 1998, A&A, 340, 508

Shepherd, D. 2003, in ASP Conf. Ser. 287: Galactic Star Formation Across the Stellar Mass Spectrum, ed. J. M. De Buizer & N. S. van der Bliek, 333–344

Shu, F. H. 1977, ApJ, 214, 488

Shu, F. H., Adams, F. C., & Lizano, S. 1987, ARA&A, 25, 23

Tilley, D. A., & Pudritz, R. E. 2005, astro-ph/0508562

Tomisaka, K. 1998, ApJ, 502, L163+

—. 2002, ApJ, 575, 306

Whitworth, A., & Summers, D. 1985, MNRAS, 214, 1

Whitworth, A. P., Bhattal, A. S., Francis, N., & Watkins, S. J. 1996, MNRAS, 283, 1061

Wolfire, M. G., & Cassinelli, J. P. 1987, ApJ, 319, 850

Yorke, H. W. 2002, in ASP Conf. Ser. 267: Hot Star Workshop III: The Earliest Phases of Massive Star Birth, ed. P. Crowther, 165–+

Yorke, H. W. 2004, in IAU Symposium, ed. M. Burton, R. Jayawardhana, & T. Bourke, 141–+

Yorke, H. W., & Sonnhalter, C. 2002, ApJ, 569, 846

This preprint was prepared with the AAS LaTeX macros v5.2.